Rhett Cheek
PHYS 3995 report, Spring Semester, 2017
Faculty supervisor: Professor Xiaochao Zheng

This spring I continued and expanded on the work I began last fall with Professor Zheng. The project that I began in the fall was to write a simulation of two hexagonal scintillator configurations, the "preshower" and the "shower". These scintillators made use of wavelength-shifting (WLS) fibers of the Y11 multi-cladding type, developed by Kuraray Co. These fibers have an emission peak at 476nm, an absorption peak at 430nm, and a diameter of approximately 1mm. The preshower configuration consists of a fiber inserted into one opening, spun around until it's in a loop, or ring, that is stacked four times, and then pulled out of the scintillator. This configuration is shown in Figure 1:

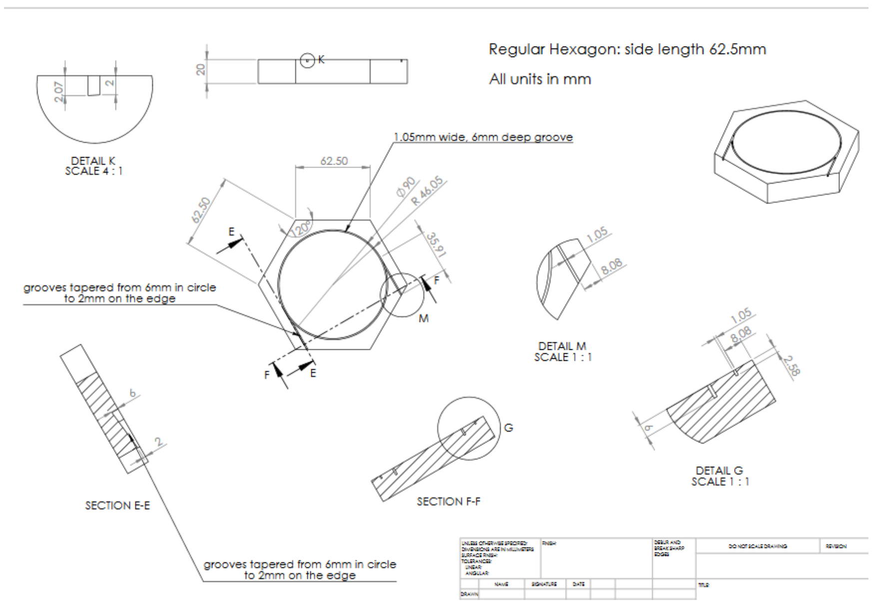

Figure 1: Preshower scintillator configuration

The shower scintillator configuration, on the other hand, has 96 fibers vertically perforating it in a pattern that is symmetric about the four quadrants of the hexagon, as shown in Figure 2:

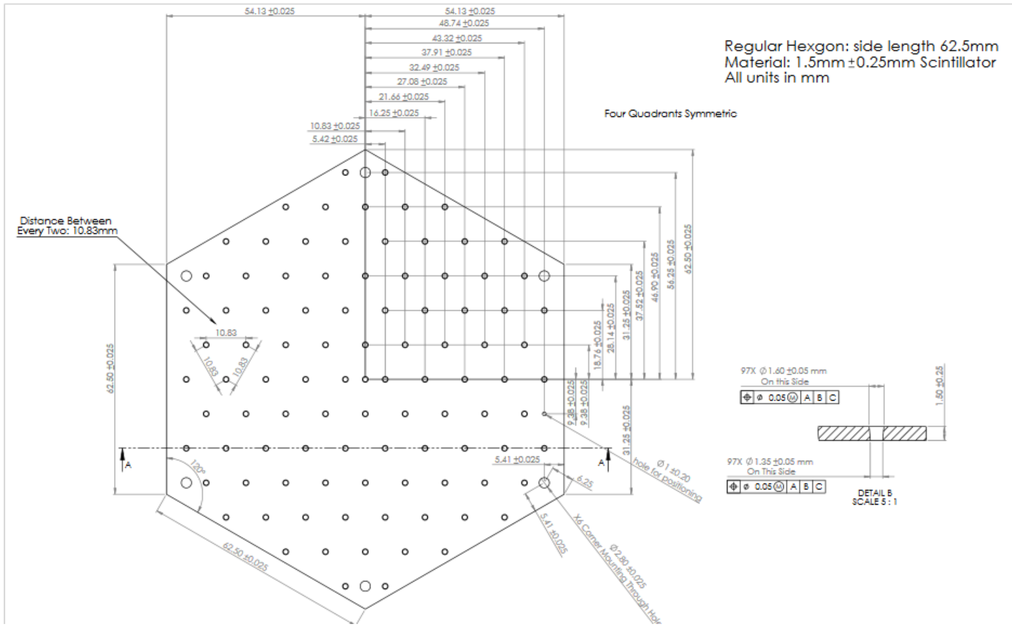

Figure 2: Shower scintillator configuration

These scintillators are used in the Electromagnetic Calorimeter in the SoLID (Solenoidal Large Intensity Device) project that is used at Jefferson Lab, which has recently acquired the capability to accelerate particles to 12GeV. This upgrade provides an opportunity to extend our understanding of nucleon spin and momentum structure by carrying out multi-dimensional precision studies of longitudinal and transverse spin and momentum degrees of freedom from SIDIS experiments with high luminosity in combination with large acceptance detectors[1]. The SoLID project's base components are arranged in two different configurations, the SIDIS (Semi-Inclusive Deep Inelastic Scattering) and the PVDIS (Parity-Violating Deep Inelastic Scattering).

The EM Calorimeter is a "shashlyk"-type (layers of lead, scintillator, and fibers) which has a total of 1800 modules of shower and 1800 modules of preshower with an area of 100cm^2 for each module, which are set behind 300 pieces of scintillator pedal detectors (SPD's) with thickness of 5mm. The

[1] *SoLID (Solenoidal Large Intensity Device) Preliminary Conceptual Design Report*, The SoLID Collaboration, July 8, 2014, p4.

energy resolution is equal to $10\%/\sqrt{E}$, it reaches a 50:1 ratio of pion suppression with electron efficiency better than 90%, and 5:1 photon suppression.

The SIDIS detector system consists of two parts: the forward-angle electromagnetic calorimeter (FAEC) detector and the large-angle electromagnetic calorimeter (LAEC) detectors. A forward-angle shashlyk is used for pion and electron separation in the FAEC; this system has momentum coverage of 0.8-7.0GeV/c. The LAEC is used for electron detection, and has a momentum range of 3.5-6.0GeV/c. One can see the SIDIS in Figure 3:

Figure 3: SIDIS diagram

The PVDIS (Figure 4) is designed to measure parity-violating asymmetries in the SoLID. It also has a “shashlyk” EM Calorimeter that is used as the trigger, in addition to assisting in pion/electron separation.

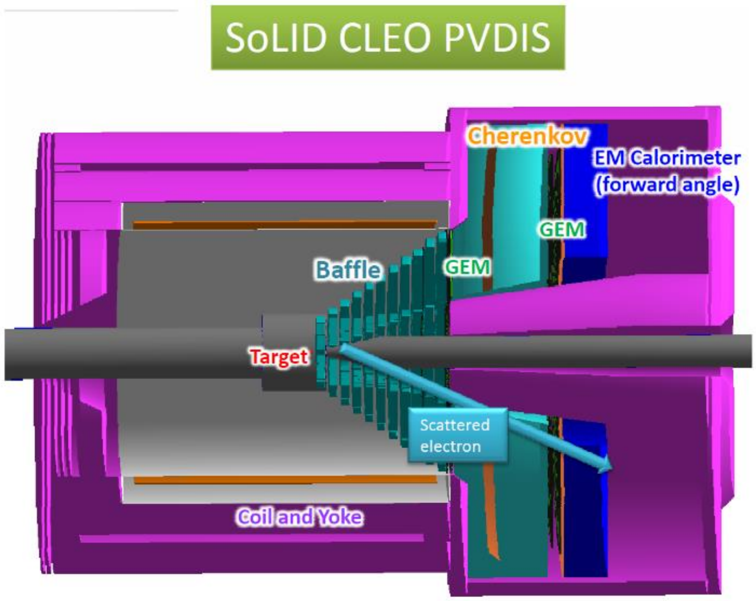

Figure 4: PVDIS diagram

To briefly summarize the situation that I started with, at the beginning of the spring semester I had a working simulation program for both the shower and preshower scintillator configurations, which tracked the positions, boundary collisions, and overall efficiency percentages of either scintillator with varying reflectivity values. The additions I've made since then are as follows: First, I wrote a program in ROOT that would plot the results of the previous semester's efficiency vs. reflectivity tests with error-bars derived from the following equation:

$$S_D = \frac{\sqrt{N*(1-e)*e}}{N} \qquad \text{(Equation 1)}$$

S_D represents the standard deviation (or error-bar width), N represents the number of photons generated in the simulation, and e represents the absorption efficiency. These results are displayed below:

Table 1 and Figure 3 describe the preshower scintillator varying the boundaries' normal reflectivity [the reflectivity when the incident angle to a boundary is less than the critical angle $\varphi_{critical} = \arcsin(\frac{1}{n_{sci}})$] while keeping the reflectivity of the total internal reflection constant at 99%:

Table 1: Absorption efficiency of preshower with variable reflectivity (non-total internal reflection)

Reflectivity	70%	75%	80%	85%	90%	95%	100%[2]
Absorption efficiency	68.13%	70.19%	73.16%	75.69%	79.69%	85.94%	97.25%

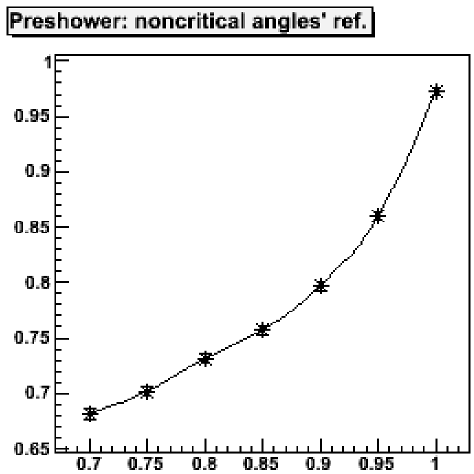

Figure 5

Table 2 and Figure 4 describe the preshower scintillator varying reflectivity when varying with the critical angle, while keeping the reflectivity of the non-total internal reflection constant at 80%:

Table 2: Absorption efficiency of preshower with variable reflectivity (total internal reflection)

Reflectivity	90%	92%	94%	96%	98%	100%[3]
Absorption efficiency	69.66%	70.20%	71.30%	71.81%	72.92%	73.20%

[2] The percentage value used 2000 photon events and reflectivity of 99.9999% due to the limitations of the .dat file size. However, the absorption efficiency is less than 100% primarily because the reflectivity of the total internal reflection is held constant at 99%.

[3] For this value I used 2000 photon events rather than 10000, and the value 99.9999% rather than 100% for the same reason as above. However, the absorption efficiency is less than 100% primarily because the reflectivity of the non-total internal reflection is held constant at 80%.

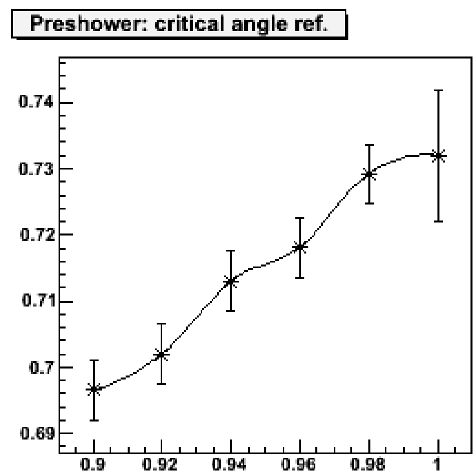

Figure 6

Table 3 and Figure 5 describe the shower scintillator varying the floor and ceiling's reflectivity, while keeping the 6 hexagonal sides' reflectivity constant at 80% and the reflectivity of total internal reflection constant at 99%:

Table 3: Absorption efficiency of shower with variable reflectivity (non-total internal reflection, floor and ceiling only)

Reflectivity	70%	75%	80%	85%	90%	95%	100%[4]
Absorption efficiency	70.51%	71.32%	72.19%	72.82%	74.25%	76.25%	88.00%

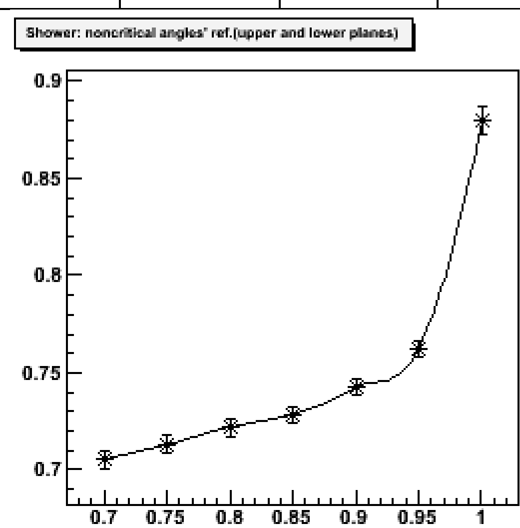

Figure 7

[4] For this value I used 2000 photon events rather than 10000 for the same reason as the note just above. However, the absorption efficiency is less than 100% primarily because the 6 hexagonal sides' reflectivity is held constant at 80% and the reflectivity of the total internal reflection is held constant at 99%.

Table 4 and Figure 6 describe the shower scintillator varying the hexagonal sides' reflectivity, while keeping the floor and ceiling's reflectivity constant at 80%, and the reflectivity of the total internal reflection constant at 99%:

Table 4: Absorption efficiency of shower with variable reflectivity (non-total internal reflection, hexagonal sides only)

Reflectivity	70%	75%	80%	85%	90%	95%	100%
Absorption efficiency	70.87%	71.81%	72.62%	72.84%	73.56%	74.08%	74.55%

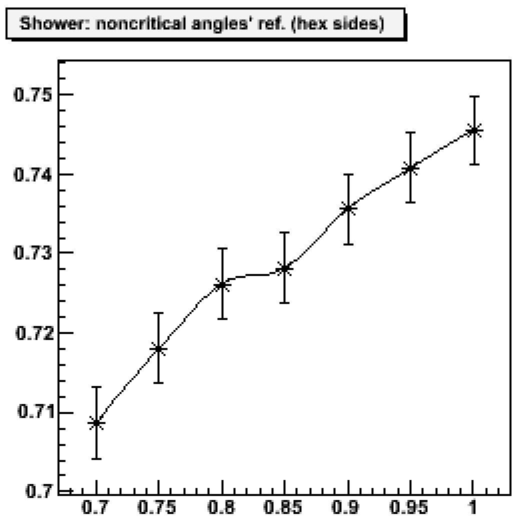

Figure 8

Table 5 and Figure 7 describe the shower scintillator varying the reflectivity when dealing with the critical angle, while keeping the reflectivity of the non-total internal reflection constant at 80%:

Table 5: Absorption efficiency of shower with variable reflectivity (total internal reflection)

Reflectivity	90%	92%	94%	96%	98%	100%[5]
Absorption efficiency	63.23%	64.50%	65.86%	67.51%	70.09%	75.85%

[5] For this value I used the value 99.999% rather than 100% and 2000 photons instead of 10000 for the same reason as the notes above. However, the absorption efficiency is less than 100% primarily because the reflectivity of the non-total internal reflection is held constant at 80%.

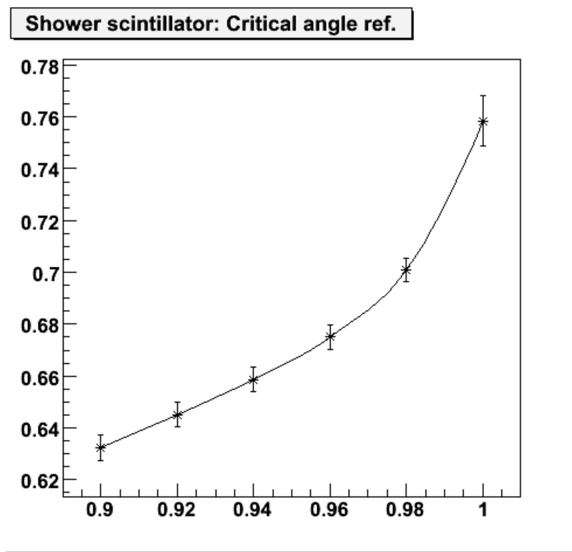

Figure 9

When viewing the graphs, one aspect to consider is the apparent visual differences in the widths of the error-bars. These differences can be attributed to the vertical axes covering differing ranges, thus the scale is different in each.

Next, I added a feature to my simulation programs that had been neglected up until that point: attenuation. This is the phenomenon where the medium that the photon passes through has a chance to absorb it. Physically, the attenuation length is a distance λ_B into a material where the probability of a particle's (in this case, a photon's) transmission through that material without being absorbed decreases to 1/e. This is shown by the Beer-Lambert Law:

$$P(x) = e^{-x/\lambda_B} \qquad \text{(Equation 2)}$$

However, it was found[6] that the distance that a photon travels through the scintillating material directly affects its attenuation length. The paper cited displays data on the dependence of the attenuation length on the light propagation in the scintillator (Figure 8) and fits it to the function (with fitting parameters A, B, and λ):

$$\lambda_B(x) = A\left(1 - e^{-x/\lambda}\right) + Bx \qquad \text{(Equation 3)}$$

[6] *Properties of Ukraine polystyrene-based plastic scintillator UPS 923A (Nuclear Instruments and Methods in Physics Research),* A. Artikov et al, available online 3 October, 2005, p 126.

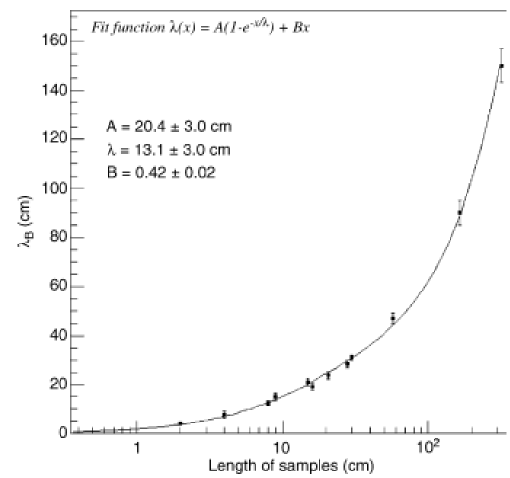

Fig. 2. Dependence of the bulk attenuation length λ_B on the light propagation in the scintillator.

Figure 10: Attenuation length and distance traveled

My simulations accounted for this by running each individual photon simulation as before, but a new variable was added to the code that kept track of how far through the material the given photon traveled. If the photon ended up escaping, no attenuation calculation is necessary to test for absorption efficiency, as escaping the scintillator and being absorbed by the medium both result in a photon lost. However, if the photon collided with and was absorbed by a WLS fiber, it would undergo an additional check to see if, at some point during its lifetime, it would have been absorbed by the medium.

First, λ_B is calculated by the photon's total distance traveled from its point of generation to the point where it collided with the fiber being used as the input "x" in Equation 3 (the values of whose fit parameters can be seen in Figure 8; for the sake of simplicity I neglected the uncertainty of those parameters in my code). Next, the values for λ_B and "x" are plugged into Equation 2; from that we see the probability of the photon transmitting in spite of attenuation. A random number from 0 to 1 is then generated, and checked against the "P" from Equation 2; if the number is equal to or lower than P, the photon is successfully absorbed by the WLS fiber, and else it is assumed to have been absorbed by the medium at some point.

The next task I worked on was to investigate the uniformity of the two scintillator configurations. By uniformity, I refer to how the absorption efficiency can be affected by the initial position of the photons. This study required that I make a few small alterations to my simulation programs: first and foremost, I changed the random-generation of the photons' positions to be user-inputs at the beginning of the program, which remain constant as it runs; in other words, the initial position remained constant, while the initial direction-vectors were still randomly generated. Next, I began the uniformity study by observing how the absorption efficiency changed when the initial position shifted along one axis. For the preshower, I held the Y-coordinate equal to 0 and the Z-coordinate equal to 0.5cm, and varied the initial X-coordinate. For the shower, I set the Z-coordinate equal to 0.05cm and Y-coordinate equal to 0.469 cm (this value is about halfway between two rows of fibers that lie near the middle of the scintillator; refer back to Figure 2), and X-coordinates vary along that axis. Figure 9 (a-b) shows the results of the preshower's uniformity along the x-axis both neglecting and including attenuation:

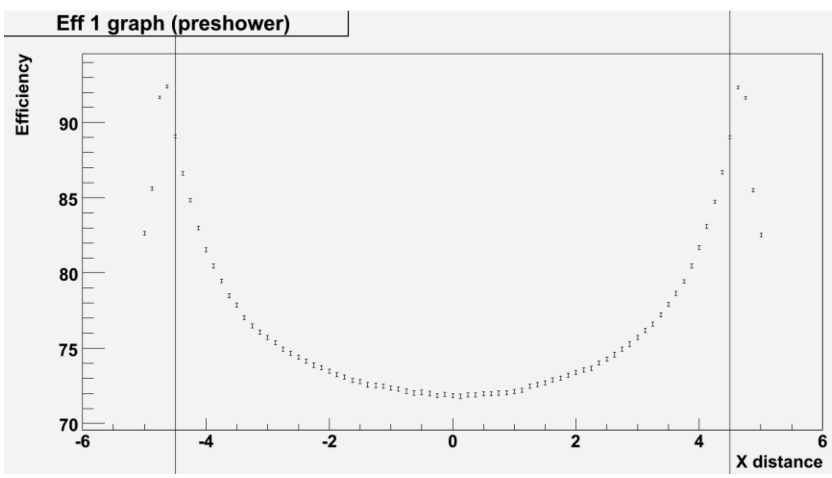

Figure 11 (a): Preshower uniformity study; attenuation neglected

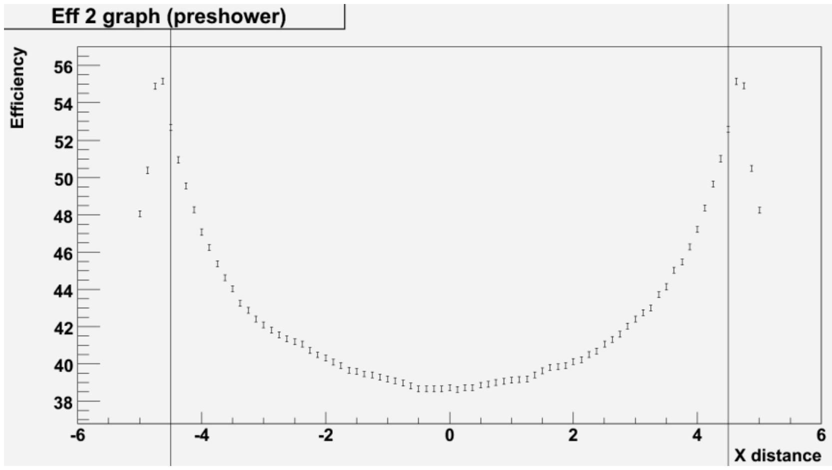

Figure 11 (b): Preshower uniformity study; attenuation included

In the figures above, the solid vertical lines represent the radius from the center where the ring of fiber in the preshower configuration lies in the given cross-section. The horizontal axis represents the displacement from the origin and the vertical axis is the percentage of photons that were absorbed. For the uniformity simulations I set the reflectivity to 90% when a photon's incident angle is less than the critical angle and 95% when it experiences total internal reflection. Figure 10(a-b)'s axes are defined identically, and the solid lines represent the locations of two rows of fibers in the shower configuration (the darker blue lines represent the first row of fibers above the center row, and the lighter cyan lines represent the X-coordinates of the fibers in the center row):

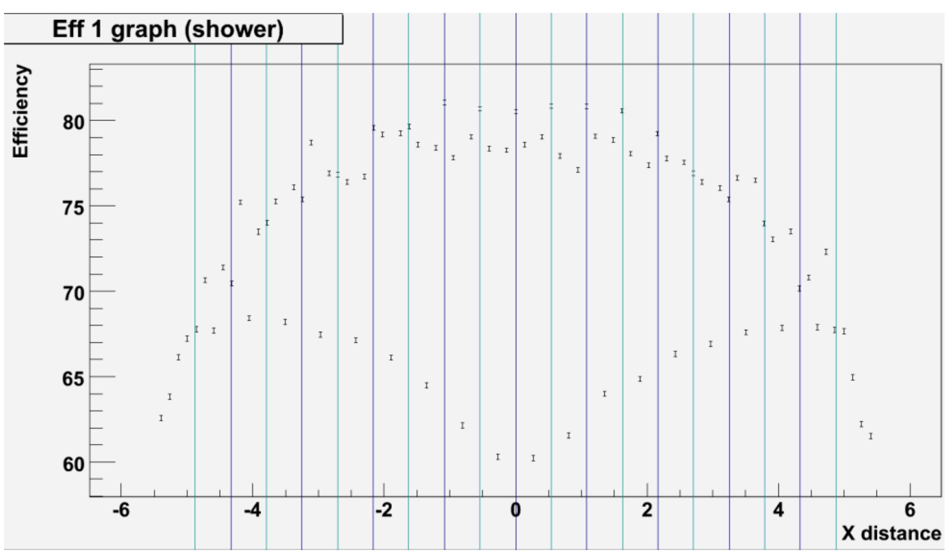

Figure 12 (a): Shower uniformity study; attenuation neglected

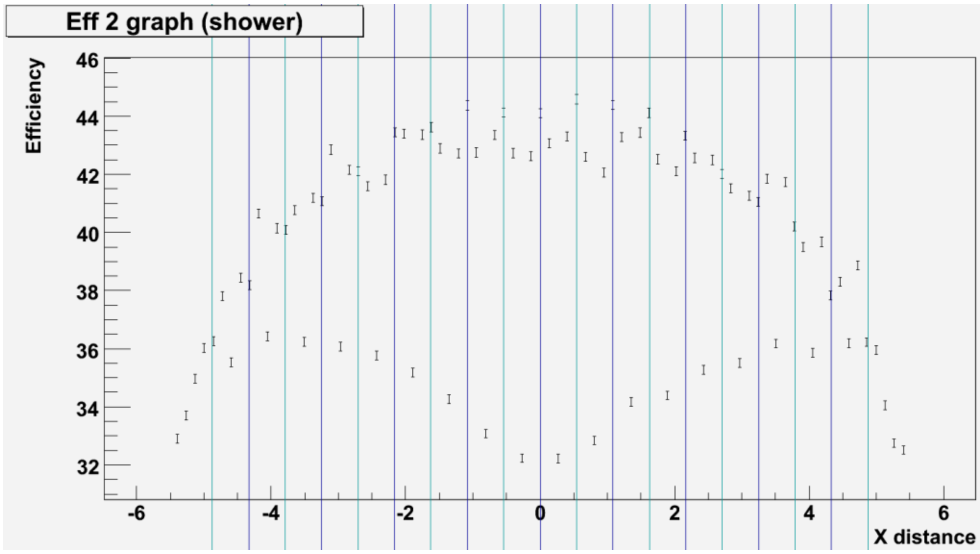

Figure 12 (b): Shower uniformity study; attenuation included

From these we observe some reasonable trends. Referring to Figure 9, the absorption efficiency increases as the initial position draws closer to the point nearest to the fibers; however the point directly under the fibers isn't the maximum. This is likely due to the fact that when directly under the fiber-ring, the solid-angle that the ring takes up is smaller than the solid angle when the initial position is displaced slightly from its path, since the efficiency reached its maximum just outside the fiber-ring. A similar occurrence is seen in Figure 10, such that when the photons are generated directly under one of the fibers, they are most likely to be absorbed since the solid-angle of the nearest fiber is greater (see Figure 11(a)). We also see a sharp decrease when the photons are generated between the fibers of both rows (see Figure 11(b)); this is likely due to the fibers' arrangement, such that many will "line up" and the photon's line of sight only allows it to see the nearer fibers. Figure 11 is arranged such that the black dot represents the photon's point of origin, and the green dots represent WLS fibers.

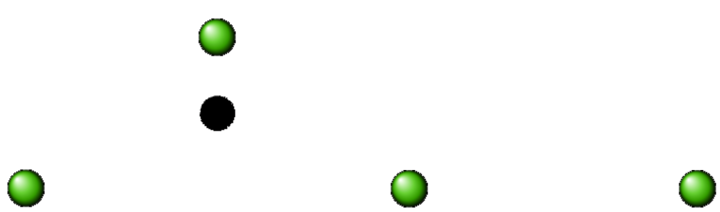

Figure 13 (a)

Figure 13 (b)

The last task I worked on was to make an alteration to the physics of reflections for both scintillator configurations. Up to this point the code was set to deal with reflection according to the Law of Reflection, as described in the fall-semester section of this report, but it was brought to my attention that due to the nature of the apparatus, diffusive reflection is a more accurate description of the photon's behavior. This means that instead of reflecting at an angle equal to the angle of incidence, the photon will instead briefly enter the boundary's material and then return with a random 3-dimensional direction vector. This applies only for incident angles less than the critical angle, so my code that accounted for diffusive reflection still applied the Law of Reflection when the photon experienced total internal reflection. I will soon repeat the uniformity study with diffusive reflection accounted for, as well as expand the study to include different values on the Y- and Z- axes to see if further insights into the absorption efficiency can be made. Figures 14-15 show some of the results of the simulation using diffusive reflection:

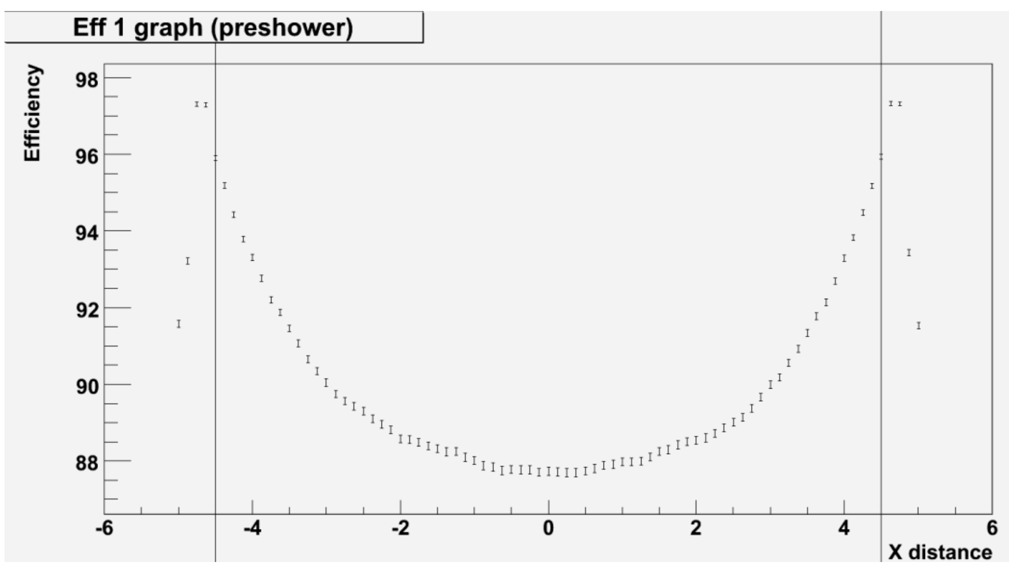

Figure 14 (a): Preshower scintillator; attenuation neglected

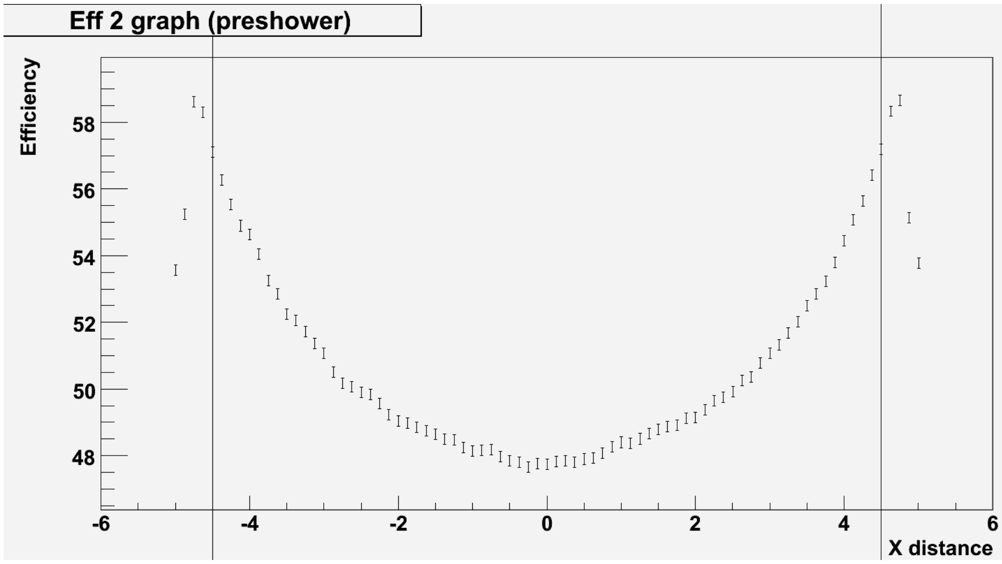

Figure 14 (b): Preshower scintillator; attenuation included

Comparing these new efficiency studies with the data provided in Figure 11, we can see that incorporating diffusive reflection into the simulation has increased the absorption efficiency provided. The overall shape of the curves remain the same as in the simulation which used the Law of Reflection for all boundary reflections, but the data shown in Figure 14 has essentially been translated upward beyond the widths of the error-bars. To compare the graphs that accounted for attenuation, the minimum for the standard reflection lies around 39.5% and its two maxima stand at roughly 55%, whereas the diffusive reflection has calculated the minimum to lie at approximately 48% and its maxima to stand just above 58%. As the Y- and Z- values were constant between the two different simulations, this yields the interesting result that the preshower scintillator's absorption efficiency may be slightly higher than initially calculated based on the Law of Reflection. Diffusive reflection also, predictably, has a smaller difference between the maxima and minimum than its earlier counterpart, down to approximately a 10% spread from 15%.

Next, I ran several points along the X-axis of the shower scintillator just as shown in Figure 12:

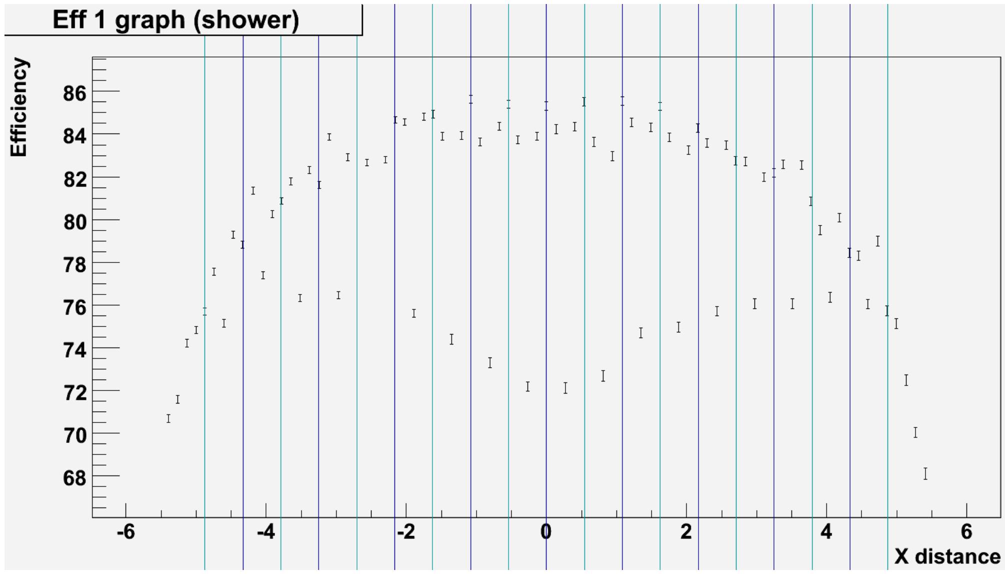

Figure 15 (a): Shower scintillator; attenuation neglected

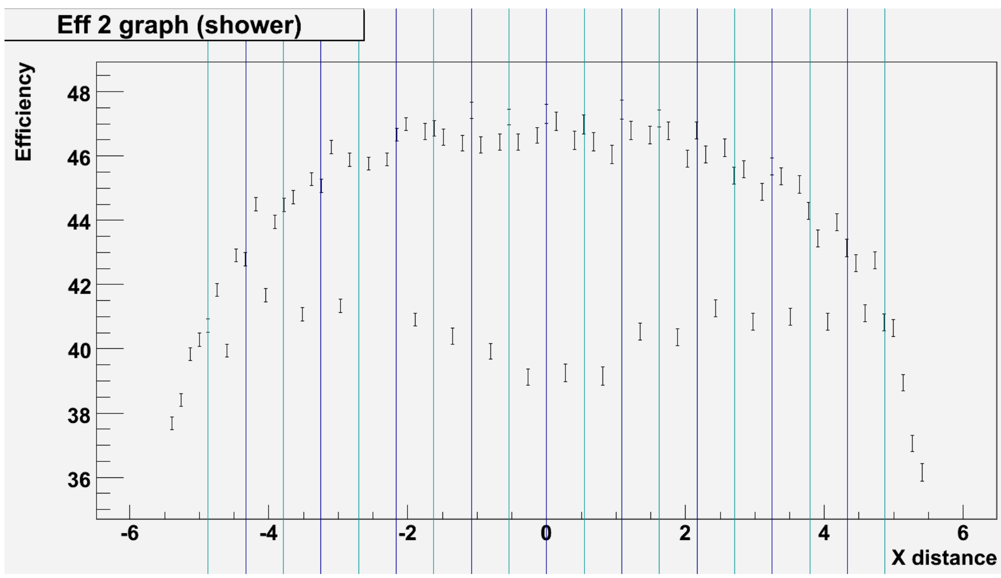

Figure 15 (b): Shower scintillator; attenuation included

Comparing Figure 15(b) with Figure 12(b), we see a similar change to the absorption efficiency as we did when we incorporated diffusive reflection into the preshower. We see the absorption efficiency has improved overall after switching into diffusive reflection: the minimum values along the "lower lip" of the data-set have moved from 32.5% in the mirror-reflection version to a little over 39% when using diffusive reflection, and the overall maximum values have moved from 44.5% to about 47%.

Diffusive reflection again, as expected, has a smaller difference between its maximum and minimum values, decreasing from a difference of 12% to 8%.

Next, I decided to test the uniformity at more varied coordinates in 3-space. For the preshower, my choice in coordinates are based on the axes shown in Figure 16, where the horizontal axis represents the x-axis and can range as far as 6.25cm from the origin, the vertical axis represents the y-axis and can range as far as 5.41cm from the origin (this distance is equal to the hexagon's side-length $*\frac{\sqrt{3}}{2}$), and the z-values represent the final dimension with possible values ranging from 0 to 2cm.

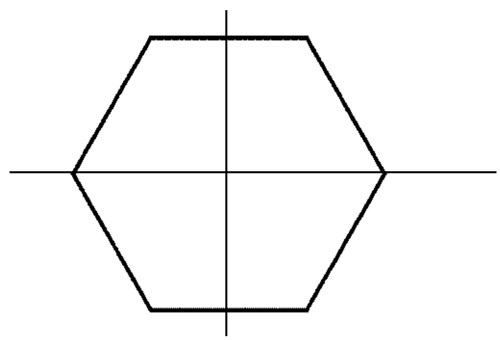

Figure 16: Axes for preshower uniformity

The following figures describe the results of my expanded uniformity study (these made use of the diffusive reflection code and set 90% reflectivity for small incident angles and 95% reflectivity for total internal reflection; for the sake of simplicity I included only the graphs that accounted for attenuation):

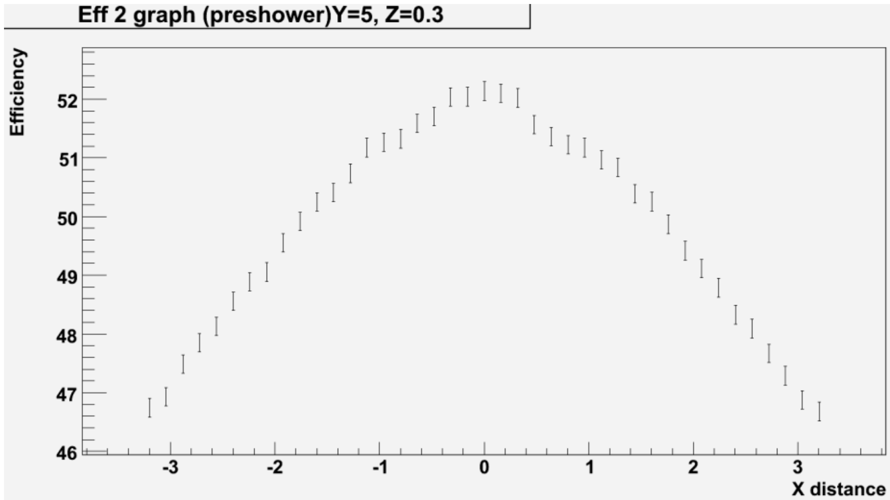

Figure 17 (a): y=5 (close to the top of the hexagon)

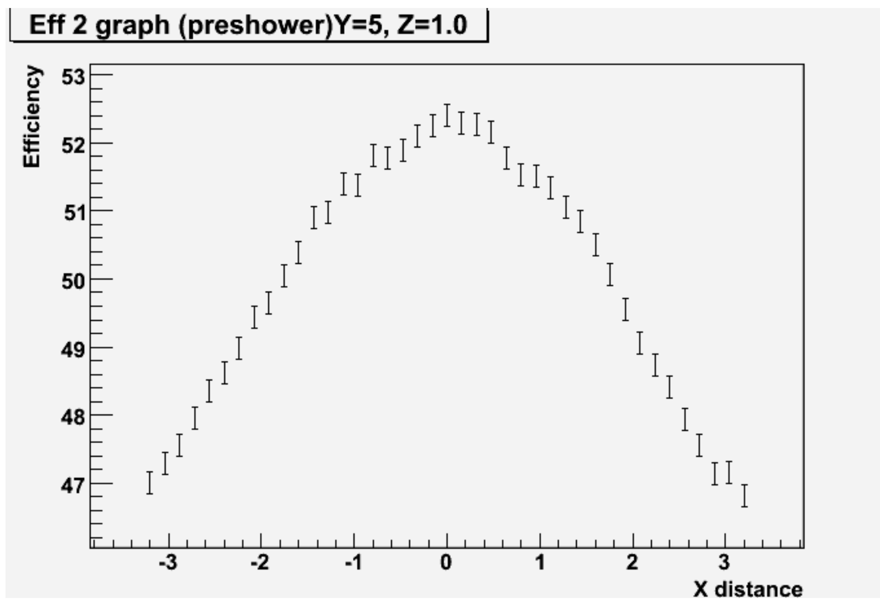

Figure 17 (b): y=5 (close to the top of the hexagon)

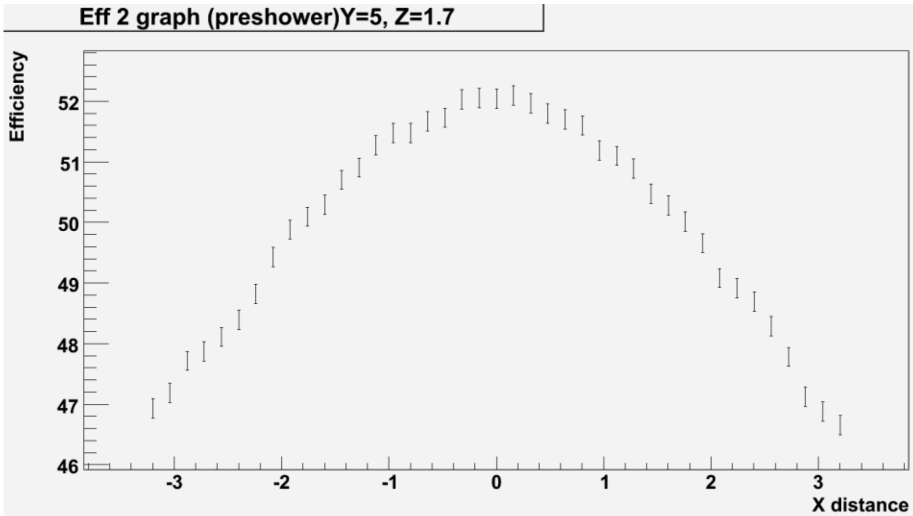

Figure 137 (c): y=5 (close to the top of the hexagon)

From Figure 17(a-c) we don't see a significant dependence on the height of the z-axis, but there does seem to be a slight increase of the maximum when Z=1.0cm as opposed to being closer to the floor and ceiling of the scintillator. The deviations are hardly outside the widths of the error-bars, however. In addition, as our run across the x-axis is beyond the perimeter of the fiber-ring, we see only one central maximum rather than two marking the positions near the locations of the fibers.

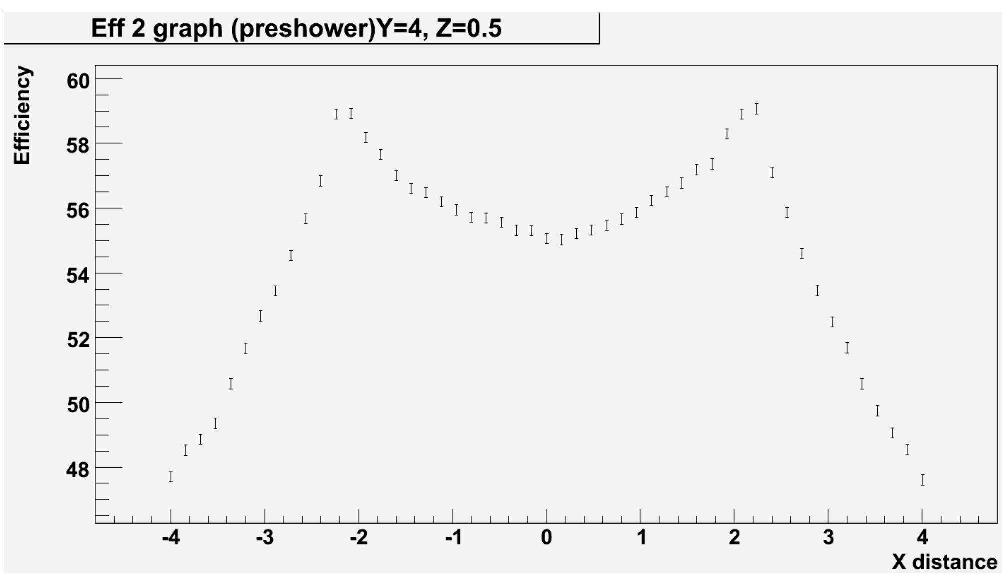

Figure 148 (a): y=4 for preshower scintillator

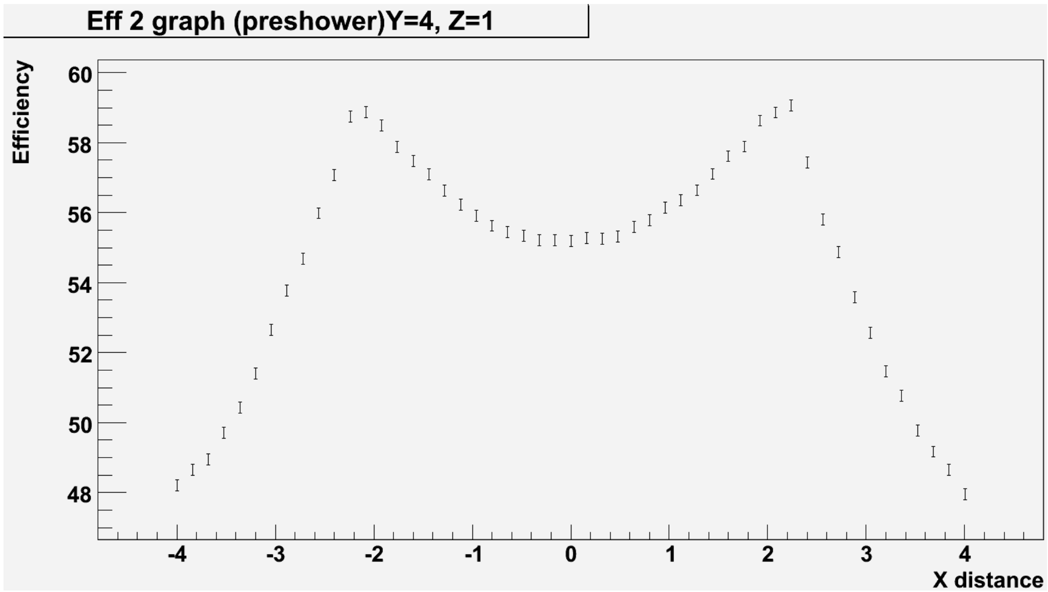

Figure 158 (b): y=4 for preshower scintillator

In Figure 18 (a-b) we see an overall increase in absorption efficiency as well as the return of two maxima symmetrically placed on the graph, indicating that the positions measured run under the ring of fiber in the preshower again. Again, the difference in the initial z-coordinate doesn't make a significant difference in the absorption efficiency. The maxima along y=4 are significantly higher than the maximum along y=5, rising from under 53% to just over 59%.

Figure 19 (a-b) shows the result generated by setting y=3 and testing two different initial z-positions:

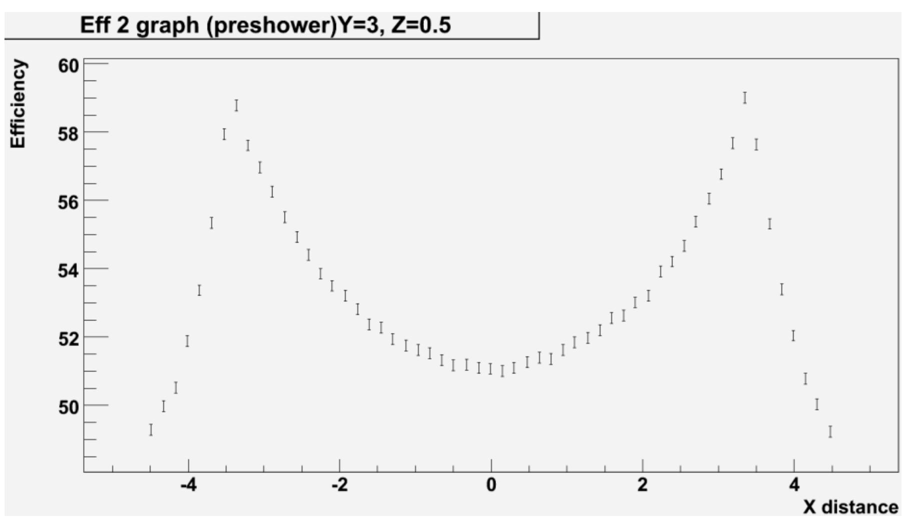

Figure 169 (a)

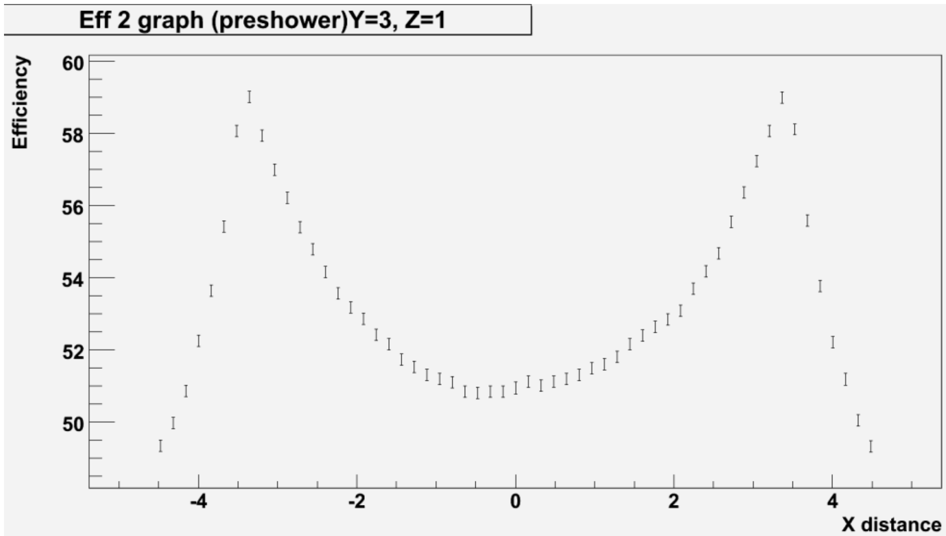

Figure 17 (b)

In Figure 19 (a-b), there isn't a significant difference in either overall shape or heights of the maxima compared to Figure 18 (a-b); Figures 20 (a-b) and 21 (a-b) are arranged similarly for y=2 and y=1 respectively. In these, the absorption efficiency again doesn't vary significantly when altering the initial y- and z-coordinates.

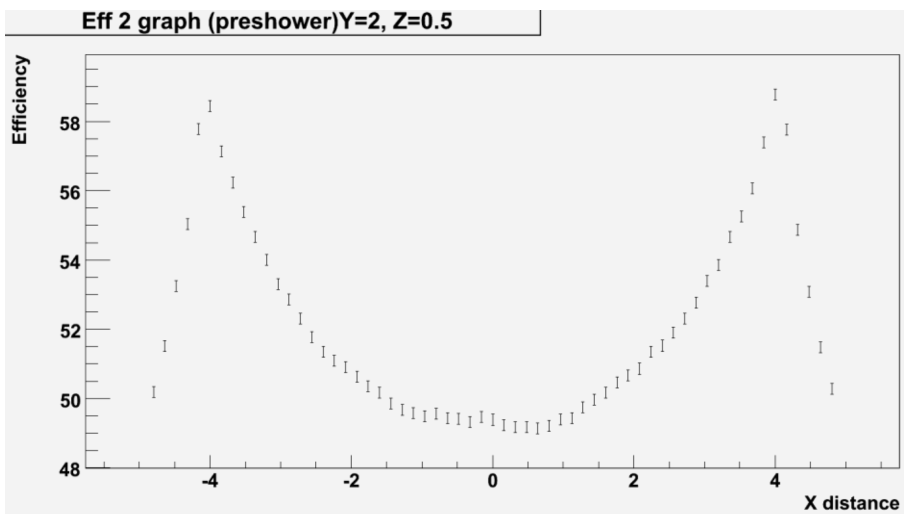

Figure 20 (a)

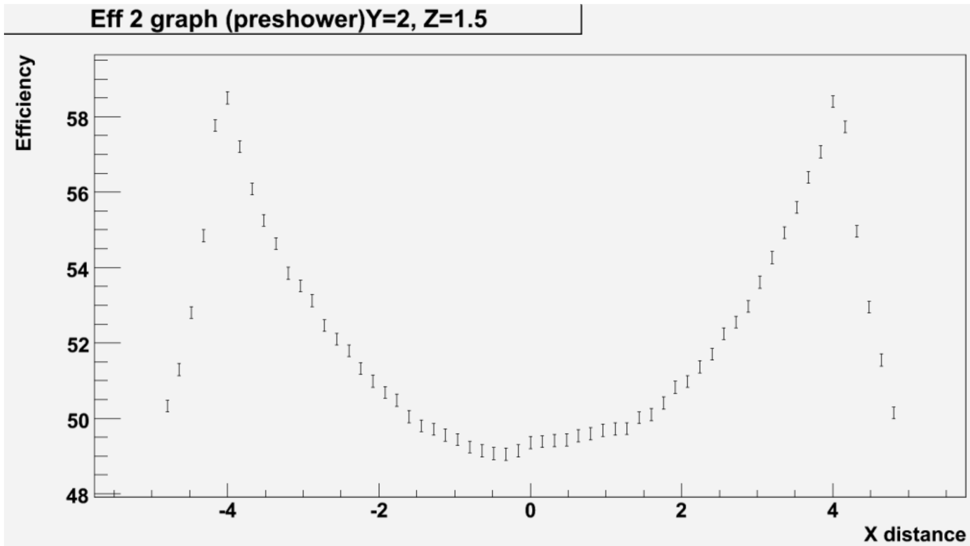

Figure 20 (b)

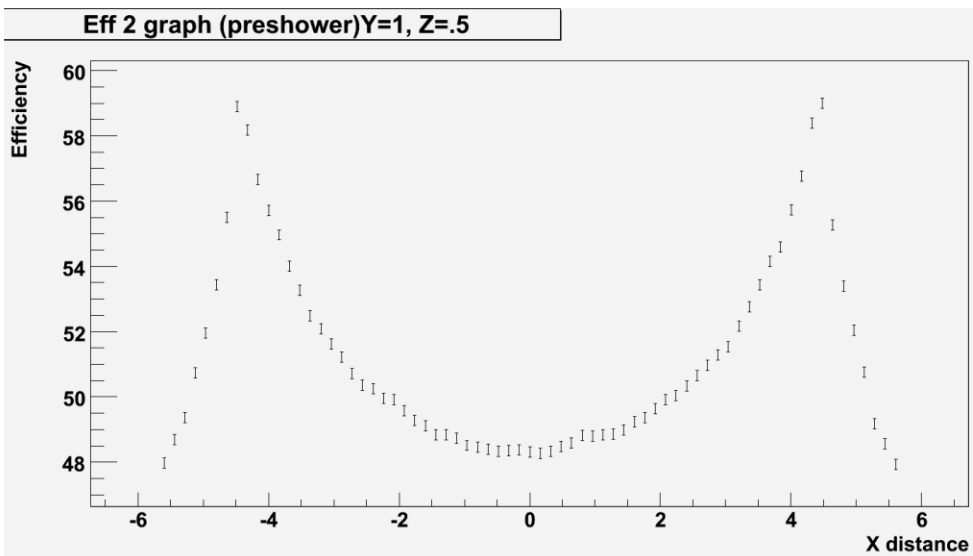

Figure 218 (a)

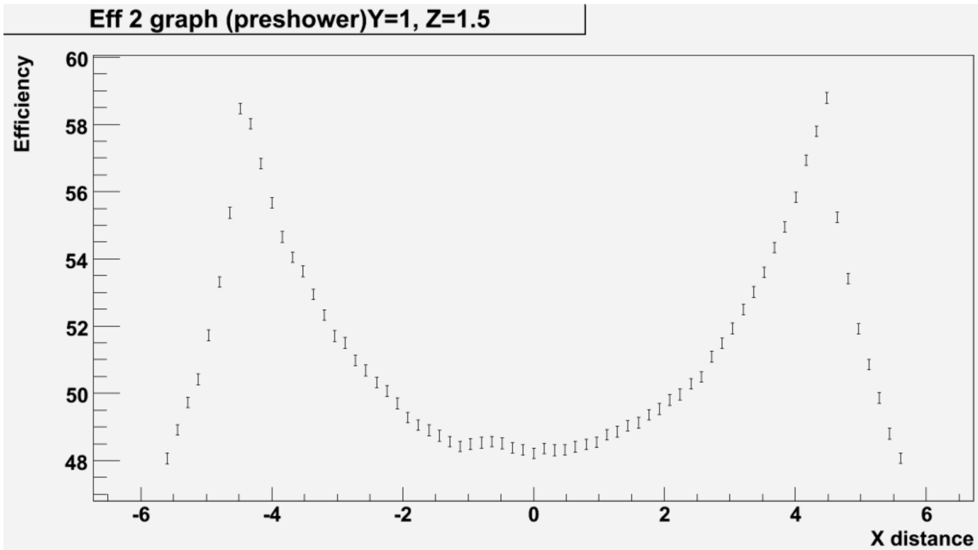

Figure 219 (b)

Overall, in the preshower scintillator the maximum initial point for absorption efficiency that I calculated is X=~3.3, Y=3, Z=1, but its value isn't significantly higher than the maxima from other y- and z- initial positions.

Next, I continue the uniformity study of the shower scintillator. To save time, I concentrated my efforts on a single quadrant of the hexagon in the same orientation as shown in Figure 2 (the coordinate system will differ slightly from that of Figure 16). My convention is to run my scan along the area where the y-coordinate lies halfway between two rows of fibers; the data shown in Figure 15 is for the section between the center row and the row just above it (refer back to Figure 2), Figures 22-26 will present data between the rows above them in ascending order, e.g. the graph titled "2nd row" was measured between the first two above the central row of fibers, the 3rd is just above that one, etc. For the sake of simplicity I used only values with positive x-coordinates and assumed that there would be symmetry along the y-axis. These figures all include attenuation and make use of diffusive reflection.

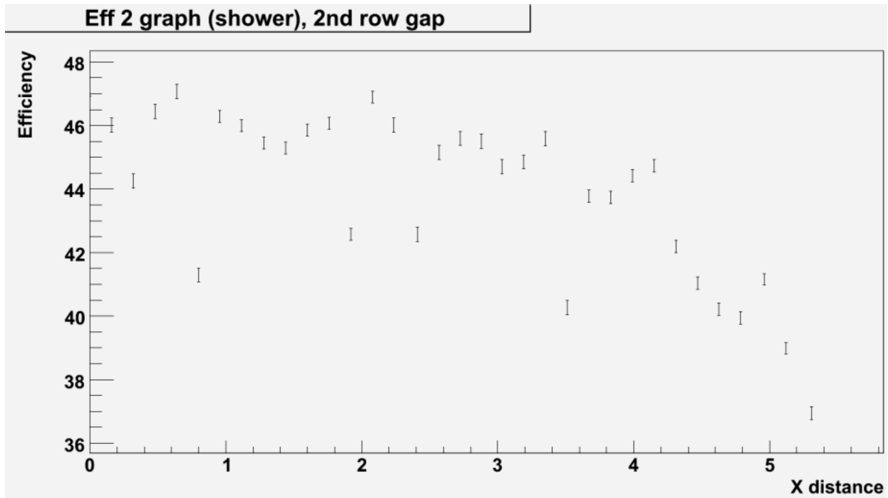

Figure 20: 2nd row (y=1.407cm)

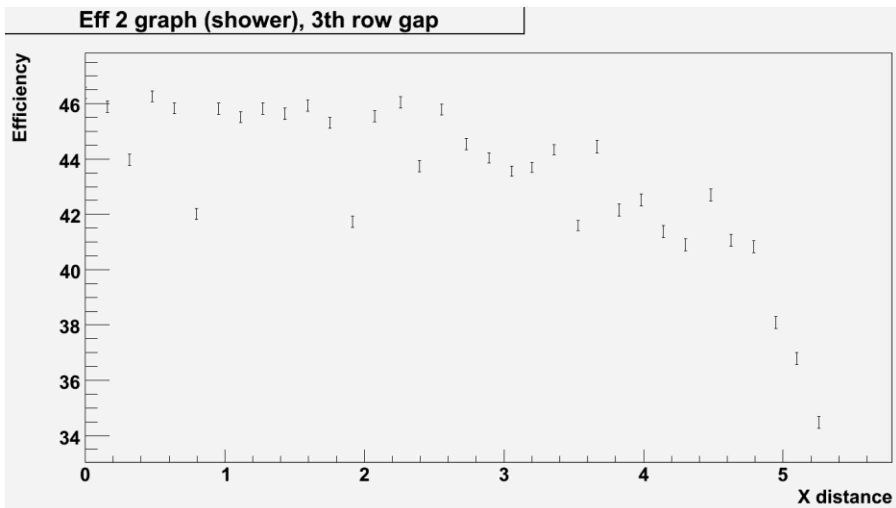

Figure 21: 3rd row (y=2.345cm)

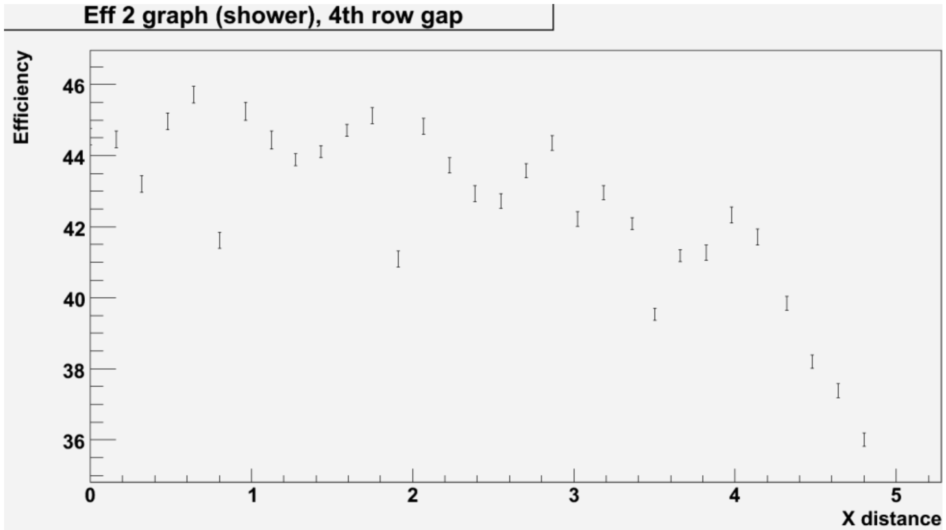

Figure 22: 4th row (y=3.283cm)

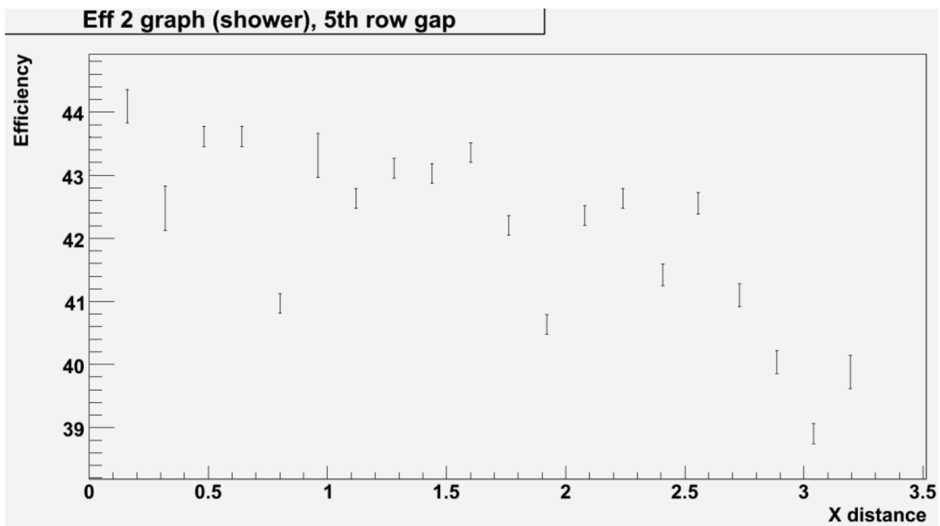

Figure 23: 5th row (y=4.221cm)

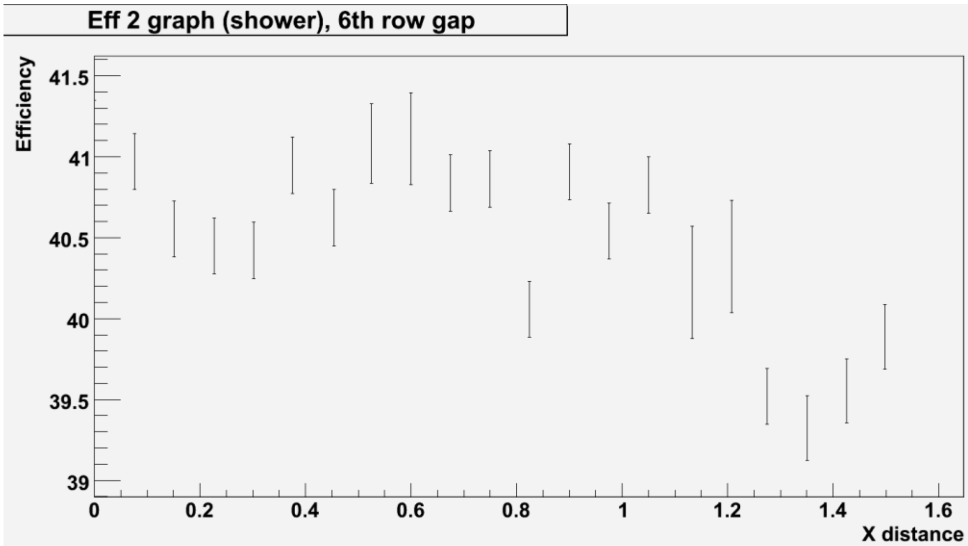

Figure 24: 6th row (y=5.1575 cm)

Based on Figures 22-26 we can see that as the point of origin deviates from y-0, the absorption efficiency begins to decrease, as the maximum absorption efficiency value from each figure decreases from approximately 47% in Figure 22, to approximately 46 in Figures 23 and 24, to approximately 44% in Figure 25, and finally to 41% in Figure 26. This decrease is reasonable as the photons will be more likely to escape before colliding with a fiber if their point of generation is close to one of the scintillator's boundaries.

In conclusion, the work done on the simulations this spring has produced a number of useful results, from those that made the simulation a more accurate representation of the physical processes involved (such as the addition of attenuation and diffusive reflection) to the detailed uniformity study that provided a significant amount of information on the absorption efficiency of the scintillator based on the point of photon generation.